

# The Responses of Magnetically Sub-Critical Cores to Shocks.

B. Vaidya<sup>1\*</sup>, T. W. Hartquist<sup>1</sup>, S. A. E. G. Falle<sup>2</sup>

<sup>1</sup>*School of Physics and Astronomy, University of Leeds, Leeds LS2 9JT, UK*

<sup>2</sup>*Department of Applied Mathematics, University of Leeds, Leeds LS2 9JT, UK*

6 May 2019

## ABSTRACT

An ideal magnetohydrodynamics (MHD) code with adaptive mesh refinement (AMR) was used to investigate the interactions of fast-mode shocks with self-gravitating, isothermal cores with mass-to-flux ratios that are somewhat below the minimum value required for gravitational collapse. We find that shock focussing produces colliding flows along the field lines that generate very high densities, even for relatively weak shocks. Self-gravity plays only a minor role in determining the highest density that is reached, but it does play a role in the subsequent evolution. The densities at comparable times differ by a factor of a few for shocks initially propagating perpendicularly or obliquely to the magnetic field in the ambient medium.

**Key words:** (magnetohydrodynamics) MHD – shock waves – stars: formation

## 1 INTRODUCTION

The importance of shock-cloud interactions for feedback in star formation has motivated a number of groups to perform 3D MHD simulations of shocks interacting with single clouds (Gregori et al. 2000; Shin et al. 2008; Kwak et al. 2009; Van Loo et al. 2010; Shelton et al. 2012). None of these simulations included self-gravity and only those of Van Loo et al. (2010) and some of those of Shelton et al. (2012) included radiative cooling. Like the two dimensional simulations of Fragile et al. (2005), Lim et al. (2005), and Van Loo et al. (2007), Van Loo et al. (2010) considered the production of cooler regions by including the thermal instability of warm phase material. Shelton et al. (2012) focussed on X-ray emission and cloud destruction rather than the cloud internal structure.

This paper concerns the effects of shocks, which are likely to be driven by the outflows of recently born stars, on cores in molecular clouds. A core is assumed to be in an isothermal magnetized equilibrium state, such as those considered by Mouschovias (1976a,b) and is magnetically sub-critical i.e. its mass-to-flux ratio is somewhat below the critical value for the core to collapse under gravity. The analysis of infrared polarization maps of some molecular clouds has shown that they contain pc scale cores that are magnetically sub-critical (Chapman et al. 2011; Marchwinski et al. 2012). We shall see that, although even quite weak shocks can produce a large increase in density, this does not lead to gravitational collapse in ideal MHD. However, self-gravity

does retard the subsequent re-expansion. We intend to include ambipolar diffusion and the Hall effect in future work (e.g., Ashmore et al. 2010).

## 2 NUMERICAL TECHNIQUE

The calculations were performed with the hierarchical adaptive mesh refinement (AMR) code, MG Falle et al. (2012). This solves the equations of ideal MHD using a second order upwind scheme with the linear MHD Riemann solver described in Falle et al. (1998) combined with the divergence cleaning technique described in Dedner et al. (2002). A hierarchy of  $N$  grids levels,  $G_0 \dots G_{N-1}$ , is used, and the mesh spacing for  $G_n$  is  $\Delta x/2^n$ , where  $\Delta x$  is the cell size for the coarsest level,  $G_0$ .  $G_0$  and  $G_1$  cover the entire domain, but finer grids need not do so. Refinement is on a cell-by-cell basis and is controlled by error estimates based on the difference between solutions on different grids i.e. the difference between the solutions on  $G_{n-1}$  and  $G_n$  determine refinement to  $G_{n+1}$ . Self-gravity is computed using a full approximation multigrid to solve the Poisson equation.

## 3 INITIAL CONDITIONS

The initial core has density  $\rho_i$ , sound speed  $c_c$  and radius  $R_i$  and is embedded in a warmer uniform medium with sound speed  $c_e = 4c_c$  and pressure  $0.9\rho_i c_c^2$ . This is implemented by defining an advected scalar,  $\alpha$ , that is unity in the cloud and zero in the surroundings. The sound speed,  $c$ , is then

\* E-mail: B.Vaidya@leeds.ac.uk (BV)

given by  $c^2 = \alpha c_c^2 + (1 - \alpha)c_e^2$ . This scalar is also used to turn off gravity in the external medium. Both the core and its surroundings are threaded by a uniform magnetic field with magnitude  $B_0$ . We use dimensionless units in which  $\rho_i = 1$ ,  $c_c = 1.0$  and the gravitation constant  $G = 1.0$ . In these units the core has  $R_i = 2.5/\sqrt{4\pi} = 0.705$  and a free-fall time of  $(3\pi/32)^{0.5}$ . For the adopted units, the initial magnetic pressure is  $B_0^2/2$  (note that we have suppressed factors of  $4\pi$  in the equations).

This initial core is not in equilibrium, but evolves into an equilibrium state provided the mass-to-flux ratio is below a critical value. This equilibrium state, which is produced by the collapse of a uniform, non-rotating, isothermal, spherical core, is the same as one of those specified by Mouschovias (1976a,b). For a zero temperature core, the critical value of mass to flux ratio is given by (Mouschovias & Spitzer 1976)

$$\frac{M_{\text{crit}}}{\Phi_{\text{crit}}} = \frac{0.53}{3\pi} \left(\frac{5}{G}\right)^{\frac{1}{2}} \quad (1)$$

Since, in case of ideal MHD, the mass-to-flux ratio does not change, we have

$$\frac{M}{\Phi} = \frac{4\rho_i R_i}{3B_0}. \quad (2)$$

We set

$$\lambda = \frac{M}{\Phi} \frac{\Phi_{\text{crit}}}{M_{\text{crit}}} = 0.707, \quad (3)$$

which gives an initial plasma  $\beta$

$$\beta_i = \frac{2\rho_i c_c^2}{B_0^2} = 0.224. \quad (4)$$

The equilibrium core has an oblate shape with an aspect ratio  $\sim 0.46$ . The maximum value of the density is 2.08 and the maximum value of  $\beta$  is 0.426.

All calculations were performed on a three-dimensional cartesian grid,  $-2 \leq x \leq 2$ ,  $-2 \leq y \leq 2$ ,  $-2 \leq z \leq 2$ , with the centre of the core at the origin. Initially 6 grids were used with a resolution of  $10^3$  on  $G_0$ , which gives an effective maximum resolution of  $320^3$  ( $225^3$  for the initial cloud). Note that  $G_0$  needs to be coarse in order to ensure fast convergence of the multigrid Poisson solver. For the evolution to the equilibrium state, free flow boundary conditions were imposed on all boundaries.

This resolution is more than adequate for the equilibrium state, but as we shall see, is not sufficient to resolve the high density region that is produced by the shock interaction. However, the code has the ability to change the number of levels during the course of the calculation, so that additional levels could be added as necessary.

#### 4 SHOCK INTERACTION

A fast-mode shock was introduced onto a grid containing the equilibrium core by setting the conditions on the  $x = 2$  plane to the postshock state for such a shock in the negative  $x$  direction with an upstream state corresponding of that of the warm medium.

We consider two cases: perpendicular ( $\theta = 90^\circ$ ) and oblique ( $\theta = 45^\circ$ ), where  $\theta$  is the angle between the shock normal and the upstream magnetic field far from the core.

For the perpendicular shocks, the equilibrium core was generated from an initial state with the magnetic field in the  $z$  direction, but for the oblique shock it was at  $45^\circ$  to the  $z$  axis.

We chose to characterize the strength of the shock by its Alfvén Mach number

$$M_a = V_{\text{shock}}/V_a, \quad (5)$$

where,  $V_{\text{shock}}$  is the shock speed in the upstream rest frame and  $V_a$  is the the Alfvén speed given by

$$V_a = B/\sqrt{\bar{\rho}}. \quad (6)$$

in our equations. This has the advantage that an oblique shock has the same speed as a perpendicular shock with the same value of  $M_a$ .

Fig. 1 shows the density for a perpendicular shock with  $M_a = 2.0$  at four times, measured from the time that the shock was introduced. As can be seen from the figure, a filamentary high density region is formed, which is highly flattened parallel to the magnetic field. In order to resolve this, it was necessary to add an extra three grid levels as the calculation proceeded to give an effective resolution of  $2560^3$  ( $900^3$  for the initial cloud). Even so, this is barely sufficient to resolve the high density region in its most compressed state. Fig. 2 shows that the oblique shock also generates a dense region.

Careful examination of the results shows that the dense region is the result of shock focussing by the density gradient at the edge of the core. A plane shock that encounters such a density gradient is refracted until its direction of propagation becomes parallel to the density gradient (much like water waves on a sloping beach). In the perpendicular case, this leads to strong focussing on the  $z = 0$  plane where the density contours have a small radius of curvature. As in a Munro jet (Birkhoff et al. 1948), this would lead to a large pressure and hence density even if there were no magnetic field, but here the velocities along the field are of the order of the post-shock Alfvén speed, which is significantly higher than the gas sound speed in the core. As a result, convergence along the field lines leads to a higher density than in the purely hydrodynamic case.

It is possible to estimate the way in which the maximum density scales with  $M_a$  and the initial  $\beta$  in the core. For a perpendicular isothermal shock, the compression (see Appendix in Yu et al. 2006) is

$$\tau = \frac{1}{2}[-\beta_0 - 1 + \sqrt{\{(1 + \beta_0)^2 + 8M_a^2\}}], \quad (7)$$

where  $\beta_0$  is the upstream  $\beta$ . The post-shock total pressure is then

$$p = \frac{B_0^2}{2}(\tau^2 + \tau\beta_0), \quad (8)$$

where  $B_0$  is the upstream magnetic field.

For the incident shock in the low density medium we have  $\beta_0 = \beta_i$  ( $= 0.224$  in our case) and we can ignore the gas pressure to get

$$\tau_i \simeq \sqrt{2M_a} \quad (9)$$

if we also ignore  $(1 + \beta_0)^2$  compared with  $8M_a^2$ . The post-shock pressure is then given by

$$p_i \simeq \tau_i^2 \frac{B_i^2}{2} \simeq M_a^2 B_i^2, \quad (10)$$

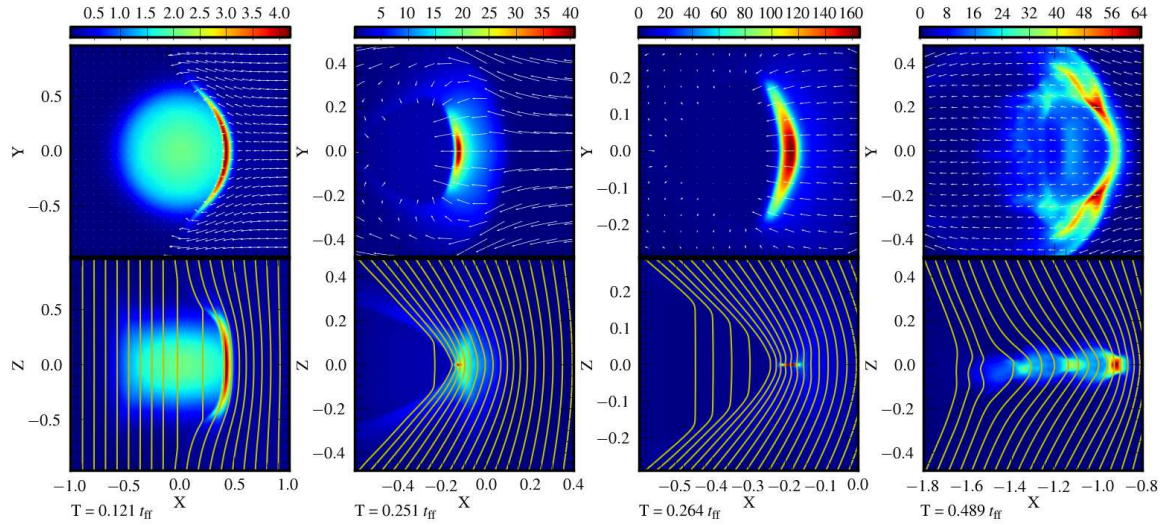


**Figure 1.** Density, velocity vectors and magnetic field lines for the perpendicular shock. Each of the four columns represents the solution at the time (expressed in terms of free fall time) indicated below the panels. The top panels show the  $z = 0$  plane and the bottom panels the  $y = 0$  plane. The white arrows in the top panels indicate velocity vectors and the solid lines in the bottom panels represent the magnetic field lines. The colorbar placed above the top panels provides the measure of core density in terms of  $\rho_i$  for each column.

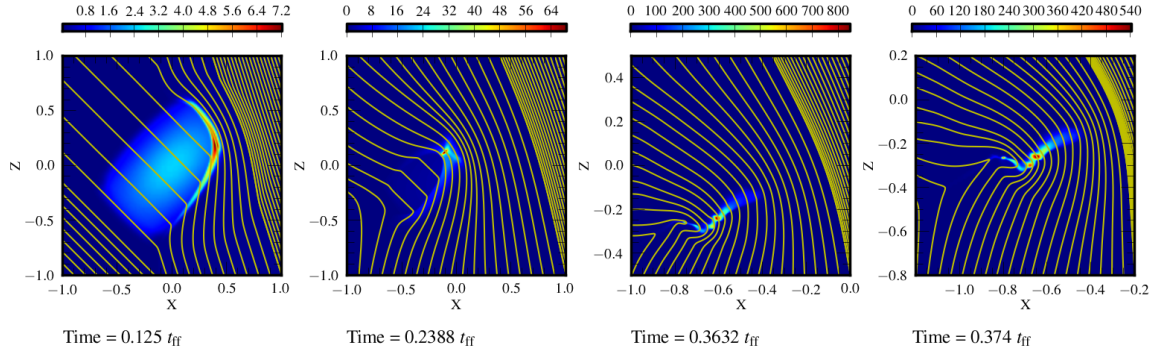


**Figure 2.** As for 1 for the  $y = 0$  plane for the oblique case.

where  $B_i$  is the initial magnetic field.

We can get a lower limit on the density behind the shock propagating into the core by assuming a perpendicular shock with post-shock pressure  $p_i$ . This is clearly a lower limit since it ignores shock convergence, the post-shock pressure is greater than  $p_i$  due to the reflected shock and the compression is greater if the shock is oblique. The shock is clearly oblique for  $z \neq 0$  since it is propagating along the density gradient, while the field in the equilibrium core is very nearly parallel to the  $z$  direction.

If  $\tau_c$  is the compression in this shock, then (8) gives

$$p = \frac{B_c^2}{2} (\tau_c^2 + \tau_c \beta_c) = p_i = M_a^2 B_i^2, \quad (11)$$

where  $B_c$  and  $\beta_c$  are the magnetic field and  $\beta$  in the core. Solving this for  $\tau_c$  gives

$$\tau_c = \frac{1}{2} \left[ -\beta_c + \sqrt{\beta_c^2 + 8M_a^2 \frac{B_i^2}{B_c^2}} \right]. \quad (12)$$

For low-temperature cores close to criticality,  $B_c \simeq B_i$ , but

although  $\beta_c < 1$ , it is not really small. Nevertheless, we shall neglect it to get

$$\tau_c = \sqrt{2M_a}. \quad (13)$$

Since the shock is actually oblique, the post-shock velocity along the field lines is of the order of the shock velocity except near  $z = 0$ . The strength of the shock is considerably increased by convergence, so that we can assume that it is strong, in which case its velocity,  $V_s$ , is given by

$$V_s^2 = \frac{p_i}{\rho_c(1 - 1/\tau_c)}. \quad (14)$$

which becomes

$$V_s^2 \simeq \frac{M_a^2 B_i^2}{\rho_c(1 - 1/\sqrt{2M_a})}, \quad (15)$$

upon substitution for  $p_i$  and  $\tau_c$  from (10) and (13).

The orientation of the shock relative to the field lines is such that the flow parallel to the field is directed towards  $z = 0$ , which means that we have two streams with velocity  $\simeq V_s$  and density  $\tau_c \rho_c$  that collide at  $z = 0$ . This produces a density of

$$\rho_{max} \simeq \tau_c \rho_c \frac{V_s^2}{c_c^2}. \quad (16)$$

Substituting for  $\tau_c$  and  $V_s^2$  from (13) gives

$$\rho_{max} \simeq 2\sqrt{2} \frac{M_a^3}{\beta_c(1 - 1/\sqrt{2}M_a)} \cdot \rho_c. \quad (17)$$

In our case we have  $M_a = 2$ ,  $\rho_c = 2.08$ ,  $\beta_c = 0.426$ , which gives  $\rho_{max} = 171$ . As we can see from Fig. 3, the maximum density is much higher than this ( $\simeq 3 \times 10^3$ ), which is presumably because we have neglected both the effect of shock convergence and the reflected shock on the strength of the shock in the core. For  $M_a = 1.5$ , the simulation gives  $\rho_{max} = 315$  (see fig. 3), whereas the multiplication of the  $M_a = 2$  simulation result for  $\rho_{max}$  by  $\zeta^3/(1 - 1/\sqrt{2}\zeta)$ , where  $\zeta = 1.5/2$ , gives  $\rho_{max} = 1577$ . This disagreement is not too surprising since the assumption of strong shocks is not valid for such low Mach numbers. It would be nice to look at larger values of  $M_a$ , but it then becomes very difficult to resolve the thickness of the high density region. All this tells us that (17) only gives a rough indication of the maximum density, but we have established that this mechanism can produce surprisingly high densities even for relatively weak shocks.

Fig. 3 also shows that the oblique shock produces densities of the same order as the perpendicular shock, which means that the effect is not dependent on a precise alignment of the shock normal with the  $z = 0$  plane. Although the oblate shape of the equilibrium core means that shock convergence is less important if the shock normal is not perpendicular to the field, this is compensated by the fact that the density is higher behind the more oblique shock in the core.

In Fig. 3 we have also plotted the maximum density for the perpendicular case with self-gravity switched off once the shock begins to interact with the core. This clearly shows that self-gravity has no effect on the evolution up to the point at which the maximum density is reached, but that it does slow down the subsequent re-expansion. In both cases the very high density does not persist for long, but the density is still substantially larger than the initial value even at the latest times.

## 5 DISCUSSION AND CONCLUSIONS

The main result of this paper is that, even for weak shocks, shock focussing leads to surprisingly large increases in density in shock-core interactions. This is entirely an MHD effect, but self-gravity is nevertheless essential to the process. The shock is focussed by the density gradient in the gravitationally bound cloud and the re-expansion of the dense region is prevented by its self-gravity.

Chen & Ostriker (2012) have argued that ambipolar diffusion in a time-dependent shock can lead to a transition from a magnetically sub-critical to magnetically super-critical state. The inclusion of ambipolar diffusion and Hall processes in future work of the interactions of shocks with cores will therefore be of considerable interest. The very large increases in density that we have found suggest that the results of Chen & Ostriker (2012), who considered plane-parallel flows only, provide rather conservative estimates of the extent to which transient effects in shocks are likely to increase the mass-to-flux ratio.

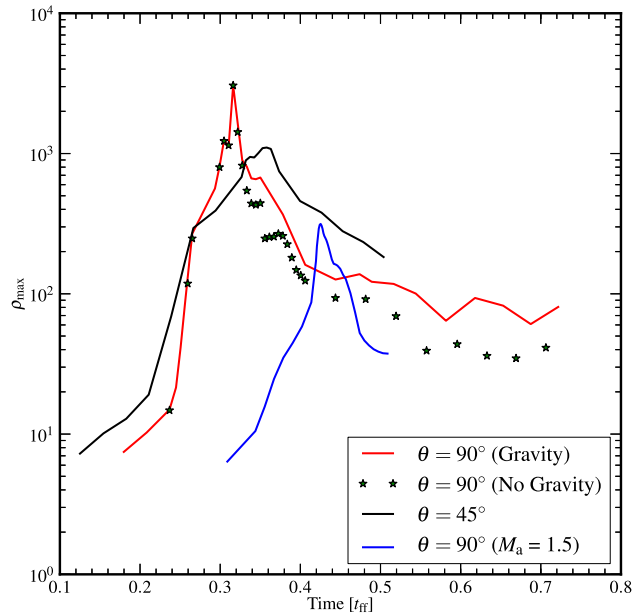


Figure 3. The maximum density as a function of time.

## REFERENCES

- Ashmore I., Van Loo S., Caselli P., Falle S. A. E. G., Hartquist T. W., 2010, *A&A*, 511, A41
- Birkhoff G., MacDougall D., Pugh E., Taylor G., 1948, *Journal of Applied Physics*, 19, 563
- Chapman N. L., Goldsmith P. F., Pineda J. L., Clemens D. P., Li D., Krčo M., 2011, *ApJ*, 741, 21
- Chen C.-Y., Ostriker E. C., 2012, *ApJ*, 744, 124
- Dedner A., Kemm F., Kröner D., Munz C.-D., Schnitzer T., Wesenberg M., 2002, *Journal of Computational Physics*, 175, 645
- Falle S., Hubber D., Goodwin S., Boley A., 2012, in Pogorelov N. V., Font J. A., Audit E., Zank G. P., eds, *Numerical Modeling of Space Plasma Shocks (ASTRONUM 2011)* Vol. 459 of *Astronomical Society of the Pacific Conference Series*, Comparison Between AMR and SPH. p. 298
- Falle S. A. E. G., Komissarov S. S., Joarder P., 1998, *MNRAS*, 297, 265
- Fragile P. C., Anninos P., Gustafson K., Murray S. D., 2005, *ApJ*, 619, 327
- Gregori G., Miniati F., Ryu D., Jones T. W., 2000, *ApJ*, 543, 775
- Kwak K., Shelton R. L., Raley E. A., 2009, *ApJ*, 699, 1775
- Lim A. J., Falle S. A. E. G., Hartquist T. W., 2005, *ApJ*, 632, L91
- Marchwinski R. C., Pavel M. D., Clemens D. P., 2012, *ApJ*, 755, 130
- Mouschovias T. C., 1976a, *ApJ*, 206, 753
- Mouschovias T. C., 1976b, *ApJ*, 207, 141
- Mouschovias T. C., Spitzer Jr. L., 1976, *ApJ*, 210, 326
- Shelton R. L., Kwak K., Henley D. B., 2012, *ApJ*, 751, 120
- Shin M.-S., Stone J. M., Snyder G. F., 2008, *ApJ*, 680, 336
- Van Loo S., Falle S. A. E. G., Hartquist T. W., 2010, *MNRAS*, 405, 151

RAS, 406, 1260

Van Loo S., Falle S. A. E. G., Hartquist T. W., Moore  
T. J. T., 2007, *A&A*, 471, 213

Yu C., Lou Y.-Q., Bian F.-Y., Wu Y., 2006, *MNRAS*, 370,  
121